Macroscopic x-ray powder diffraction imaging reveals Vermeer's discriminating use of lead white pigments in Girl with a Pearl Earring

De Meyer, S.; Vanmeert, F.; Vertongen, R.; Van Loon, A.; Gonzalez, V.; Delaney, J.; Dooley, K.; Dik, J.; Van der Snickt, G.; Vandivere, A.

DOI
10.1126/sciadv.aax1975

Publication date
2019

Document Version
Final published version

Published in
Science Advances

Citation (APA)
De Meyer, S., Vanmeert, F., Vertongen, R., Van Loon, A., Gonzalez, V., Delaney, J., Dooley, K., Dik, J., Van der Snickt, G., Vandivere, A., & Janssens, K. (2019). Macroscopic x-ray powder diffraction imaging reveals Vermeer's discriminating use of lead white pigments in Girl with a Pearl Earring. *Science Advances*, *5*(8), Article eaax1975. https://doi.org/10.1126/sciadv.aax1975

CHEMICAL PHYSICS

Macroscopic x-ray powder diffraction imaging reveals Vermeer's discriminating use of lead white pigments in *Girl with a Pearl Earring*

S. De Meyer[1]*, F. Vanmeert[1], R. Vertongen[1], A. Van Loon[2,3], V. Gonzalez[2,4], J. Delaney[5], K. Dooley[5], J. Dik[4], G. Van der Snickt[1,6], A. Vandivere[3], K. Janssens[1]

Until the 19th century, lead white was the most important white pigment used in oil paintings. Lead white is typically composed of two crystalline lead carbonates: hydrocerussite [$2PbCO_3{\cdot}Pb(OH)_2$] and cerussite ($PbCO_3$). Depending on the ratio between hydrocerussite and cerussite, lead white can be classified into different subtypes, each with different optical properties. Current methods to investigate and differentiate between lead white subtypes involve invasive sampling on a microscopic scale, introducing problems of paint damage and representativeness. In this study, a 17th century painting *Girl with a Pearl Earring* (by Johannes Vermeer, c. 1665, collection of the Mauritshuis, NL) was analyzed with a recently developed mobile and noninvasive macroscopic x-ray powder diffraction (MA-XRPD) scanner within the project *Girl in the Spotlight*. Four different subtypes of lead white were identified using XRPD imaging at the macroscopic and microscopic scale, implying that Vermeer was highly discriminatory in his use of lead white.

INTRODUCTION

Girl with a Pearl Earring is an iconic oil painting created by the 17th century artist Johannes Vermeer in the collection of the Mauritshuis, The Hague (Fig. 1A). One of the most well-documented (and often recurring) features in Vermeer's paintings is the delicate blend between light and shadow (*1*, *2*). In *Girl with a Pearl Earring*, there is a stark contrast between the bright facial tones and the dark background, while within the *Girl*'s face, a smooth transition from light to dark is present. A pigment used by Vermeer to accentuate this contrast is lead white. Historically, lead white was the most important white pigment used in easel paintings until the 19th century, after which zinc white and titanium white became more dominant (*3*). Before the 19th century, lead white was usually produced by the stack process, in which sheets of lead were exposed to vinegar and horse manure (*4*). The resulting lead white is typically composed of two crystalline compounds: cerussite (C) ($PbCO_3$) and hydrocerussite (HC) [$2PbCO_3{\cdot}Pb(OH)_2$] (*5*). Adjustments to the synthesis parameters or additional postsynthesis treatments may cause the mass ratio of these two phases to change, leading to a pigment with different physico-chemical and, consequently, optical properties (*6*). Differences in the lead white ratio have an influence on the opacity and brightness of the pigment, while a change in particle size will substantially influence a pigment's covering power, making it either more transparent or opaque. Consequently, investigating the lead white ratio provides insight into both the production process of the pigment and the optical effects the artist intended to express, which is highly relevant information for art historians and conservators. Previous microscopical analysis has already shown that Vermeer (and other artists, e.g., Grünewald) used different types of lead white in their paintings (*7*, *8*).

In the recent past, several synchrotron-based methods of analysis have been used to gain insight into the various types of lead white pigments used by painters. With high-resolution x-ray diffraction, it is possible to precisely estimate the crystal phase composition of paint samples; high lateral resolution x-ray powder diffraction (μ-XRPD) allows for spatial imaging of crystalline phases present in complex multilayered cross sections of paint samples (*6*, *9*). However, the major drawback of these two techniques is that they require invasive sampling on the original painting, an undertaking that either is not permitted or is limited to those locations on the painting

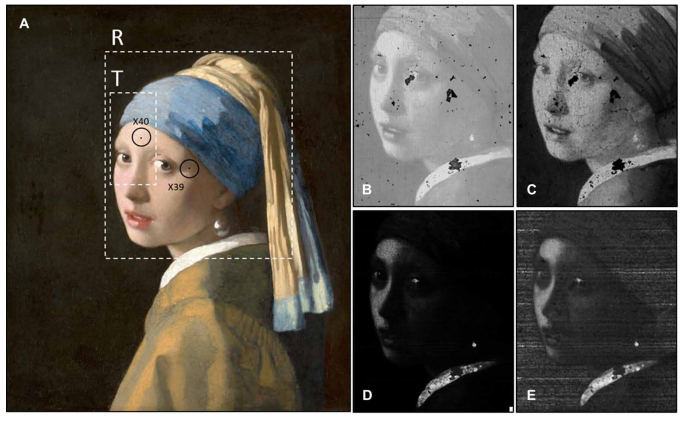

Fig. 1. Comparison of various macroscopic imaging techniques. (**A**) Visual photograph of *Girl with a Pearl Earring* marked with the areas scanned with transmission (T) and reflection MA-XRPD (R). The locations where the paint cross sections X39 and X40 were taken are marked with a circle. (**B**) MA-XRF distribution for Pb-L and (**C**) MA-XRF distribution for Pb-M. (**D**) NIR reflectance imaging spectroscopy distribution displaying the integrated area of the narrow —OH absorption feature associated with hydrocerussite, centered near 1447 nm, in reflectance units. (**E**) Pseudo absorption of the narrow —OH absorption feature. Photo credit: René Gerritsen, Art & Research Photography and Mauritshuis.

[1]AXES, Department of Chemistry, University of Antwerp, Groenenborgerlaan 171, 2020 Antwerp, Belgium. [2]Conservation and Science Department, Ateliergebouw Rijksmuseum, Museumstraat 1, 1071 XX Amsterdam, Netherlands. [3]Paintings Conservation, Mauritshuis, Plein 29, 2511 CS The Hague, Netherlands. [4]Department of Materials Science and Engineering, Delft University of Technology, Mekelweg 2, 2628 CD Delft, Netherlands. [5]National Gallery of Art, Constitution Avenue Northwest, Washington, DC 20565, USA. [6]Conservation Studies, University of Antwerp, Blindestraat 9, B-2000 Antwerp, Belgium.
*Corresponding author. Email: steven.demeyer@uantwerpen.be

where the paint layer already shows signs of damage. Solely relying on a limited number of samples of micrometric dimensions to obtain information on a painting's material composition as a whole introduces problems of representativeness.

To bypass the problems of invasive sampling and its representativeness, noninvasive and nondestructive mobile methods of analysis, capable of imaging paintings on the macroscopic scale, have been developed in recent years. Macroscopic x-ray fluorescence (MA-XRF), for example, has been extensively used as an imaging technique to obtain two-dimensional (2D) elemental distributions (*10*, *11*). While MA-XRF is capable of visualizing the presence of the element lead both at the surface and deeper within the painting, it is unable to differentiate between compounds of a similar or identical elemental composition that feature a different crystal structure, such as cerussite and hydrocerussite. Macroscopic imaging spectroscopy techniques that have been used in the field of cultural heritage to provide information on the molecular level include macroscopic reflectance Fourier transform infrared (MA-rFTIR) spectroscopy (4000 to 400 cm^{-1}) and near-infrared (NIR) reflectance imaging spectroscopy (14,285 to 4000 cm^{-1}) (*12*, *13*). Unfortunately, the applicability of MA-rFTIR is strongly limited when a varnish layer is present, while NIR reflectance imaging spectroscopy cannot detect the presence of cerussite. Raman spectroscopy has been previously used to investigate the presence of lead carbonates (*14*). The application of Raman spectroscopy on oil paintings is, however, limited due to the interference from molecular fluorescence signals originating from the oil.

A relatively unknown technique in the field of cultural heritage is macroscopic x-ray powder diffraction (MA-XRPD). MA-XRPD scanning provides the option of faster imaging compared to previously developed portable XRPD instruments. These portable devices can be considered as an adequate alternative to sampling for investigating immovable objects such as mural paintings or outdoor sculptures, but their long acquisition time (20 to 60 min) limits their use to point-by-point investigations (*15*, *16*). While its microscopic analog (μ-XRPD) is mostly used at synchrotron facilities to examine minute paint samples, MA-XRPD exploits low-power x-ray sources and can be used for noninvasive in situ analysis (*17*, *18*). MA-XRPD combines the high specificity and imaging capabilities of μ-XRPD with the macroscopic scale of the aforementioned techniques, making it a suitable method for differentiating and quantifying various types of lead white on large artworks. MA-XRPD has been used in the recent past for visualizing the distributions of two types of chrome yellow, $PbCrO_4$ and $PbCr_{1-x}S_xO_4$, on the painting *Sunflowers* by Vincent Van Gogh (*19*). It has also been used for obtaining quantitative information on a 15th century illuminated manuscript (in transmission mode) and a small mock-up painting (in reflection mode) (*20*, *21*).

This study aims to shed light on the different types of lead white Vermeer used in *Girl with a Pearl Earring* and to demonstrate the capabilities of MA-XRPD for providing quantitative information on different paint layers in a multilayered painting. For this purpose, next to the painting as a whole, two paint cross sections were analyzed at a synchrotron facility by means of μ-XRPD, facilitating a direct comparison and interpretation of the macroscopic and microscopic data. The MA-XRPD analysis was conducted as part of an interdisciplinary project to examine *Girl with a Pearl Earring*. The research project *The Girl in the Spotlight* is a joint project of the Mauritshuis and a team of internationally recognized specialists working within the collaborative framework of the Netherlands Institute for Conservation + Art + Science + (NICAS). Within this project, the painting was analyzed with a multitude of techniques, including MA-XRF, NIR reflectance imaging spectroscopy, and MA-XRPD.

The MA-XRPD scanner was used in two different measurement modes: transmission and reflection. In transmission mode (MA-tXRPD), information on the entire stratigraphy of the painting is obtained, while reflection mode (MA-rXRPD) is more sensitive to compounds located close to the surface of the painting (fig. S1). A small angle between the incident x-ray beam and the surface of the painting is chosen, resulting in a shallow probing depth that varies strongly depending on the paint matrix: from 10 μm or less for a paint matrix dominated by heavy elements (Pb, Hg, …) up to 50 μm or less for a matrix mainly composed of light elements (C, O, Ca, Si, …). The advantage of this technique is that only diffraction signals from the superficial layers will substantially contribute to the diffraction pattern. Information from deeper within the paint stratigraphy is blocked by the upper layers. By exploiting the complementary nature of these two measurement modes, a clear estimation of the buildup and composition of the various lead white–containing layers could be attained. This information allowed us to formulate a hypothesis about the way Vermeer overlaid opaque and transparent paint layers to create the face of the *Girl*.

RESULTS

MA-XRF analysis of the face

MA-XRF imaging was used to obtain elemental maps, including those of Pb-L (Fig. 1B) and Pb-M (Fig. 1C), that visualize the presence of lead throughout the painting. The Pb-L x-ray fluorescence signals are higher in energy and come from deeper within the lead white paint stratigraphy (<200 μm), while the lower energy Pb-M signals originate from layers close to the surface (<10 μm). The Pb-L distribution shows the omnipresence of lead throughout the painting (with the exception of some retouchings). The Pb-M distribution, on the other hand, shows a lower lead abundance in the background area, meaning that most of the lead is located beneath the surface. The stratigraphy of a painting typically consists of a ground layer on which the artist would apply one or more paint layers and a varnish layer. In this case, the low Pb-M and high Pb-L intensity in the dark background implies the presence of a lead-rich ground layer. The Pb-M distribution also shows that there are superficial lead-containing compounds present in every part of the face.

NIR reflectance imaging spectroscopic analysis of the face

NIR reflectance imaging spectroscopy (967 to 1680 nm) enabled mapping of hydrocerussite within the painting, down to (but not including) the ground layer by using the first overtone of —OH stretching (fig. S2) (*22*). This narrow absorption feature is centered near 1447 nm and, if present, was fitted with a Gaussian function. Figure 1D shows the integrated area of the hydroxyl group absorption. To more readily compare the NIR reflectance imaging results with those obtained with MA-XRPD and MA-XRF, we converted the map from reflectance (R) to pseudo absorbance (A') units by applying the function $A' = \log(1/R)$ (Fig. 1E). The clear contrast in Fig. 1E between the left, hydrocerussite-rich and the right, hydrocerussite-poor part of the face already suggests a relevant difference in composition between both parts of the face. However, since the Pb-M intensity (Fig. 1D) in these areas is similar, the data suggest that the left side of the face contains significantly more hydrocerussite

at the paint surface than the right side. Another lead-containing compound must be present in the right part of the face, balancing the total amount of lead in both areas. This hints at the presence of either a cerussite-rich paint and/or of secondary Pb-containing product(s) caused by the degradation of lead white. Detection of hydrocerussite by NIR reflectance in the background areas is hindered by a high level of noise (see Fig. 1E), likely caused by the presence of carbon black, which substantially absorbs the hydrocerussite —OH band.

Synchrotron μ-XRPD analysis of paint cross sections

Two paint samples were taken from the *Girl*, prepared as cross sections and analyzed with μ-XRPD at beamline P06 of the PETRA III facility: one sample (X40; see Fig. 1) originated from a bright pink flesh tone area, rich in hydrocerussite and a second sample (X39; see Fig. 1) came from a shadow tone area, poor in hydrocerussite. The sample locations were carefully selected on the basis of the results obtained from the macro-imaging techniques to support and complement the findings of MA-XRPD. In Fig. 2, the distribution maps of the most relevant identified crystalline phases are shown for both samples. The scan parameters and the dimensions of the scanned area for both cross sections are listed in table S1.

In sample X39, from a shadow tone on the cheek of the *Girl*, three layers could be identified by μ-XRPD. The top layer (a_1) is very thin (~10 μm) and appears to be rich in lead white with some traces of vermillion (cinnabar, HgS). Beneath this upper paint layer, a second layer (a_2) consisting mainly of palmierite ($PbSO_4{\cdot}K_2SO_4$) is present: This is a secondary reaction product that can be associated with the degradation of lead white in the presence of lake pigment substrates that contain sulfur (*23*, *24*). Below these two thin layers, the ground layer (b, ~100 μm in thickness) is present, which contains a mixture of mostly chalk (calcite, $CaCO_3$) with some lead white (both hydrocerussite and cerussite).

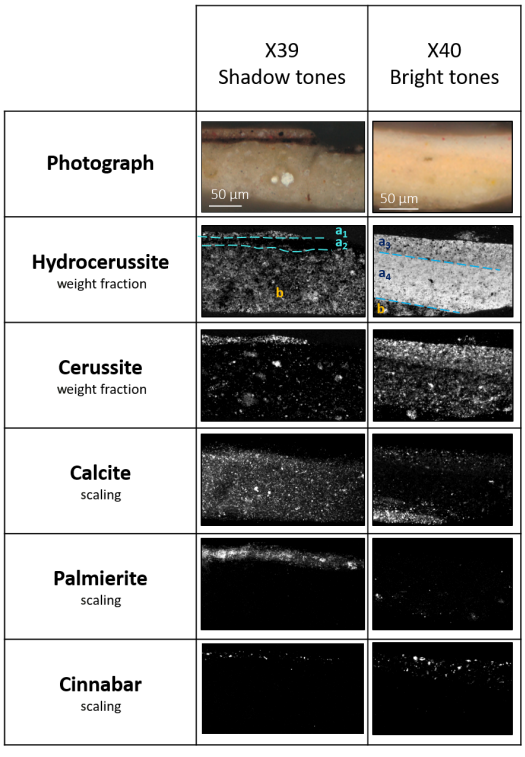

Fig. 2. Crystalline phase distributions obtained by μ-XRPD for two paint cross sections collected from the *Girl*'s face. For hydrocerussite and cerussite, the weight fractions were calculated in every pixel of the image. For calcite, palmierite, and cinnabar, a scaling parameter is displayed instead to improve the qualitative readability of the maps. Brighter areas indicate a higher weight fraction or scaling parameter value. The intensity was scaled independently for each image to improve readability: Intensities should not be directly compared. The scan parameters and size of the scanned areas are shown in table S1.

To determine whether Vermeer used the same lead white paint for the upper paint layers and ground layers, we required a quantitative approach. By using whole-pattern fitting, the relative abundance of hydrocerussite within the lead white was calculated as $w_{HC}/(w_{HC} + w_C)$ by using the relative weight fractions (w) of hydrocerussite (HC) and cerussite (C). The relatively large size of the hydrocerussite and cerussite particles with respect to the incoming x-ray beam leads to diffraction patterns that are dominated by intense diffraction spots; this prevents us from reliably calculating the weight fractions of the different components in each individual pixel. Averaging the XRPD response of multiple grains over tens or hundreds of pixels, however, leads to a cumulative powder-like diffraction pattern with a more uniform orientation, significantly increasing the accuracy of the calculated weight fraction to within an error of 10%. By repeating this procedure for every layer, the $w_{HC}/(w_{HC} + w_C)$ ratio for every lead white–containing layer in the stratigraphy can be obtained. In the case of sample X39, a ratio value of 0.48 ± 0.05 is obtained for the top layer (a_1), while the ground layer (b) contains a lead white paint with a $w_{HC}/(w_{HC} + w_C)$ ratio of 0.83 ± 0.08.

A similar qualitative and quantitative analysis was made for sample X40, taken from a bright area on the forehead of the *Girl*. Initially, only two separate layers were observed with μ-XRPD: a fairly thick (~100 μm) top layer (a) consisting of mostly lead white with some vermillion, while underneath part of the ground layer (b) is present, consisting of a mixture of mostly calcite and some lead white. In this sample, no palmierite was found, aside from a few grains deep inside layer (a_4). After calculating the weight fractions of the lead carbonates, it became clear that layer (a) can be further subdivided in a thin top layer (a_3, ~30 μm) and a thicker bottom layer (a_4, ~70 μm). The upper layer has a $w_{HC}/(w_{HC} + w_C)$ ratio of 0.65 ± 0.07, while the lower layer features a ratio of 0.79 ± 0.08. [In this sample, the ratio for the ground layer (b) could not be accurately estimated because of the limited amount of lead white present in the small part of this layer that was analyzed.] A clear contrast between the layers a_1 and a_2, found in sample X39, is visible in the distribution maps of hydrocerussite and cerussite (Fig. 2). These microscopic distribution maps are consistent with the hypothesis that Vermeer painted the left (bright) and right (shadow) parts of *the Girl*'s face using a different (combination of) lead white paint.

Reflection mode MA-XRPD analysis of the face

Figure 3 (B to F) shows the distributions of the compounds identified by means of MA-rXRPD (see table S1 for details of the reflection scan). It is clear that hydrocerussite and cerussite are prominently present in the upper layers of the face, whereas in the dark background of the painting, calcite and palmierite are the dominant species. However, a small amount of hydrocerussite and cerussite is still detectable in the dark background areas. Furthermore, vermillion was used extensively in the *Girl*'s lips and only sparsely in the pink flesh tones of her face. Closer inspection of the hydrocerussite and cerussite images reveals some clear differences: The presence of

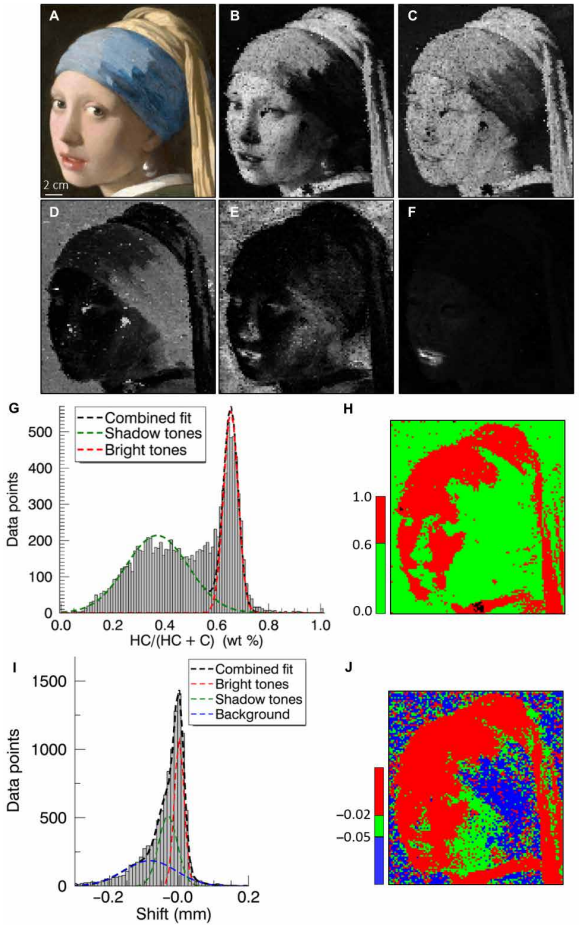

Fig. 3. Results obtained with MA-XRPD reflection mode. (**A**) Optical photograph of the analyzed area. (**B** to **F**) Distribution images obtained with reflection MA-XRPD showing the scaling parameter for every pixel. Higher scaling parameter values are represented by a brighter color. (B) Hydrocerussite, (C) cerussite, (D) calcite, (E) palmierite, and (F) cinnabar. (**G**) Histogram for the $w_{HC}/(w_{HC} + w_C)$ ratios. The black dashed line represents the combined contribution of both Gaussian curves. (**H**) Corresponding RGB image for (G). (**I**) Histogram for the average depth of hydrocerussite relative to the average depth of cerussite. (**J**) Corresponding RGB image for (I). Images were scaled independently of each other: Intensities should not be directly compared. Photo credit: René Gerritsen, Art & Research Photography and Mauritshuis.

hydrocerussite is more prominent on the left (bright) side of the face than on the right (shadow) side, while cerussite has a mostly uniform distribution across her entire face.

Again, the weight fractions for both components were calculated to obtain a more quantitative understanding of the lead white ratios in the scanned area. Another advantage MA-rXRPD has over synchrotron μ-XRPD is that a relatively large x-ray beam (1 mm × 0.2 mm) is used for imaging. In this way, many crystals are being irradiated at once, resulting in powder-like patterns. The weight ratio calculated for each individual pixel will therefore be less prone to errors than is the case for the μ-XRPD data; however, an error of approximately 5 to 10% on the individual weight fractions should still be considered, especially in the dark background areas that only show low quantities of both hydrocerussite and cerussite.

In Fig. 3G, a histogram of $w_{HC}/(w_{HC} + w_C)$ for every pixel of the scanned area is shown. A clear bimodal distribution is visible: a broad distribution with a mean $w_{HC}/(w_{HC} + w_C)$ ratio of 0.37 (as estimated using the Gaussian curve shown in green) and a narrow distribution with a mean $w_{HC}/(w_{HC} + w_C)$ ratio of 0.65 (as estimated using the Gaussian shown in red). When visualizing the location of these two groups in the distribution image (Fig. 3H), it becomes apparent that they are linked to distinct features in the *Girl*'s face. The broad distribution with a lower mean $w_{HC}/(w_{HC} + w_C)$ ratio (0.37) is correlated with the shadow tones in the face and the background of the painting, while the narrow group with a higher mean $w_{HC}/(w_{HC} + w_C)$ ratio (0.65) matches with the brighter tones. The large distribution width of the lead white ratios in the background originates from the large error induced by the small quantities of both hydrocerussite and cerussite in this region and because of strongly differing contributions of the hydrocerussite-rich ground layer to the collected diffraction data. Where the thickness of the upper paint layer varies laterally, either a larger (where the paint layer is thin) or smaller (where the paint layer is thick) volume of the ground layer will be probed, increasing the width of the Gaussian distribution in the shadow region.

These findings strongly suggest that there might be a cerussite-rich layer present at the surface in the shadow areas that causes the low $w_{HC}/(w_{HC} + w_C)$ ratio, as evidenced in sample X39. Further evidence to support this claim can be found by considering the displacement parameter of the XRPD patterns obtained after whole-pattern fitting. This displacement is indicative of a slightly larger or smaller distance of the diffracting material relative to the paint surface; this information can be used to roughly estimate the relative depth below the painting surface of individual compounds within a multilayered stack of paint strata (*20*). This phenomenon is visualized and explained in more detail in fig. S3. In this case, the average depth of the center of mass for hydrocerussite is considered relative to the average depth of the center of mass for cerussite. Figure 3I shows a histogram for the depth of hydrocerussite relative to that of cerussite for every data point in the scan. The negative values indicate that, within the probed region, the average depth at which cerussite is located is closer to the surface of the painting than the average depth at which hydrocerussite is present. The histogram data can be described by three Gaussian contributions: one corresponding to no difference in depth (red), another representing a medium depth difference (green), and a third one showing a large depth difference (blue). These three distributions are shown in the RGB map (Fig. 3J). The bright parts of the *Girl*'s face correspond to a relative depth of approximately 0, meaning that cerussite and hydrocerussite are located at a similar depth within the probed region. When taking the μ-XRPD results from this region (sample X40; Fig. 2) into account, it can be assumed that only the upper layer was probed by MA-rXRPD in which hydrocerussite and cerussite are homogeneously mixed. For the shadow part of the *Girl*'s face, the relative depth becomes more negative, indicating that cerussite is, on average, located closer to the surface than hydrocerussite. When compared to the corresponding μ-XRPD results (sample X39; Fig. 2), it can indeed be envisioned that not only the very thin upper layer but also the poorly attenuating organic layer below and the upper part of the hydrocerussite-rich ground layer were probed with MA-rXRPD. The attenuation coefficient of the upper layer is estimated to be 50 to 100 $cm^2\ g^{-1}$ (dependent on the organic fraction within the upper layer: binding medium, red lakes, carbon black, …), which translates to a probing depth of approximately 10 to 20 μm, i.e., larger than the size of the upper layer itself. In the shadows, the center of mass of hydrocerussite will

therefore be deeper within the sample than in the bright parts. In addition, in the dark background, the relative depth is negative. This is consistent with the presence of cerussite in the upper glaze layer (Fig. 3G), a thick black organic layer and a hydrocerussite-rich ground layer. The prior observations suggest that the paint layer buildup in the bright areas differs from the shadow areas of the *Girl*'s face and from the dark background area surrounding the face: In the shadow tones, a thin upper layer containing cerussite-rich lead white is present, while in the bright areas, hydrocerussite and cerussite are homogeneously mixed.

Transmission MA-XRPD analysis of the face

In transmission mode (MA-tXRPD), the x-ray beam probes the entire depth of the paint stratigraphy. The resulting diffraction patterns are consequently dominated by diffraction signals from crystalline materials with a high abundance in the probed volume (usually components from the thick ground layer) and a high scattering power (usually Pb- and Hg-containing pigments). Thus, MA-tXRPD is less sensitive than MA-rXRPD for identifying superficial compounds (present in thin paint layers or resulting from degradation phenomena at the surface), as the obtained diffraction signals are averaged out over the entire depth of the painting. Hence, MA-tXRPD is well suited for obtaining quantitative information on the composition of the ground layer.

The details of the MA-tXRPD scan are summarized in table S1. By means of MA-tXRPD, only hydrocerussite, cerussite, and calcite are detected in the analyzed area (Fig. 4, A to D). These three compounds make up most of the ground and paint layers and therefore dominate the transmission diffraction data. In Fig. 4D, the calcite shows a (mostly) uniform presence over the entire analyzed area, confirming the presence of a calcite-rich ground layer. Although the exact thickness and buildup of the paint layers are only precisely known at the locations where samples were taken, it is assumed that the bright and shadow areas feature a stratigraphy similar to their corresponding samples.

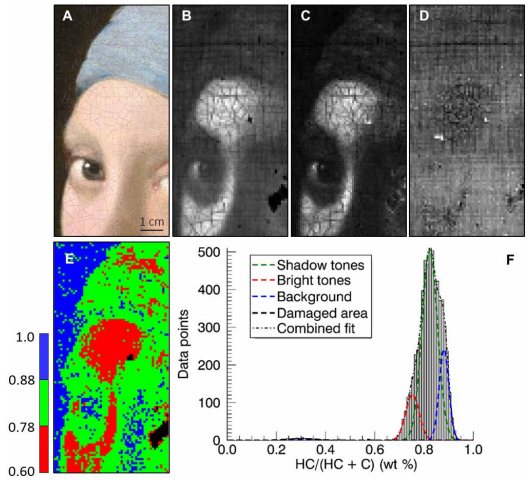

Fig. 4. Results obtained by MA-tXRPD. (**A**) Optical photograph of the analyzed area (**B** to **D**) Distribution images obtained with MA-tXRPD showing the scaling parameter for every pixel. Higher scaling parameters are represented by a brighter color. Images were scaled independently of each other: Intensities should not be directly compared. (B) Hydrocerussite, (C) cerussite, and (D) calcite. (**E**) False color image and (**F**) Histogram showing the $w_{HC}/(w_{HC} + w_C)$ ratio. Photo credit: René Gerritsen, Art & Research Photography and Mauritshuis.

The MA-tXRPD images of hydrocerussite and cerussite (Fig. 4, B and C) suggest that more lead white paint is present in the bright parts of the face (such as in the forehead) than in the shadow tones of the face (e.g., around the eyes) and the dark background. The $w_{HC}/(w_{HC} + w_C)$ ratio in these three areas only seems to vary slightly, ranging from an average value of 0.75 ± 0.05 in the bright tones to 0.82 ± 0.06 in the shadow tones and 0.88 ± 0.04 in the background (Fig. 4E). The histogram of the $w_{HC}/(w_{HC} + w_C)$ ratio can be resolved into four separate contributions: a pixel group (red) representing the bright tones, a second group (green) corresponding to the shadow areas, a third group (blue) linked to the background, and finally, a black group indicating a damaged area under the *Girl*'s left eye.

At first sight, these findings seem to conflict with the results derived from the MA-rXRPD data. The lead white paint used for the bright areas of the face was found to be rich in hydrocerussite [$w_{HC}/(w_{HC} + w_C) = 0.65 \pm 0.06$] in reflection mode compared to transmission mode (0.75 ± 0.05). For the shadow tones and background, lead white rich in cerussite was found in reflection mode (0.37 ± 0.20), while in transmission mode, a lead white rich in hydrocerussite was found for the shadow tones (0.82 ± 0.06) and for the background (0.88 ± 0.04). It is, however, important to take into account that MA-rXRPD probes the paint stratigraphy in a superficial manner (i.e., the upper 5 to 10 μm for concentrated lead white paint), while the complete paint stratigraphy (including the ca. 150-μm-thick ground layer) is probed in transmission mode. Thus, the fairly thin (10 μm or less) cerussite-rich upper paint layer in the shadow tones only has a minor contribution to the transmission diffractogram, resulting in a $w_{HC}/(w_{HC} + w_C)$ ratio that largely mirrors that of the hydrocerussite-rich ground layer. On the other hand, in the bright areas of the face, the contribution of the thick top layer [with $w_{HC}/(w_{HC} + w_C) = 0.65 \pm 0.06$] is much more substantial. Given the fact that this thick layer has a lower $w_{HC}/(w_{HC} + w_C)$ ratio than the ground layer, the resulting $w_{HC}/(w_{HC} + w_C)$ ratio of the entire stratigraphy in the bright areas will be lower than in the shadow areas.

DISCUSSION

By combining the transmission and reflection $w_{HC}/(w_{HC} + w_C)$ ratios obtained with XRPD imaging at the macroscopic and microscopic scale, a lead white layer structure can be proposed for three different regions in *Girl with the Pearl Earring*: the bright and shadow flesh tone areas and the background area. Furthermore, the μ-XRPD analyses allow us to verify our assumptions based on the MA-XRPD data and elucidate the possibilities and limitations of this technique (Fig. 5 and Table 1).

The dark background was analyzed with MA-tXRPD to gain insight into the composition of the ground layer. The lead white in the ground layer is heavily diluted within a calcite matrix, and the MA-tXRPD results show that the average ratio of chalk to lead white is 0.75 ± 0.08, a composition that is assumed to be constant throughout the entire painting. The average $w_{HC}/(w_{HC} + w_C)$ ratio of the ground layer is estimated to be 0.88 ± 0.04. In reflection mode, it was shown that the paint layers in the background contain a very small amount of cerussite-rich lead white. The contribution of these paint layers to the $w_{HC}/(w_{HC} + w_C)$ ratio obtained in transmission mode can therefore be neglected. Therefore, we consider the $w_{HC}/(w_{HC} + w_C)$ ratio obtained in transmission mode for the background to be a good estimate of the lead white composition used for the ground layer of the painting.

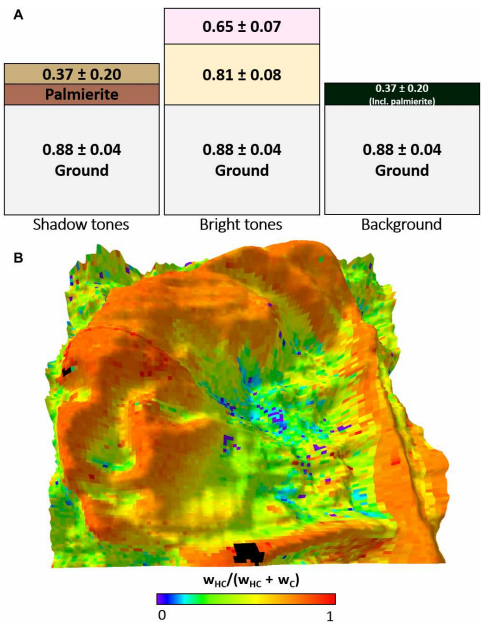

Fig. 5. Combined results of macro- and micro-XRPD. (**A**) Proposed stratigraphy for the lead white paint and ground layers based upon the MA-XRPD (transmission and reflection) and μ-XRPD data for the shadow flesh tones, bright flesh tones, and dark background. In each layer, the corresponding $w_{HC}/(w_{HC} + w_C)$ ratio is indicated. Layer thickness is not to scale. (**B**) 3D image showing the relation between $w_{HC}/(w_{HC} + w_C)$ ratio (ranging from 0 to 1, black indicates areas without lead white) and the relative depth of hydrocerussite compared to cerussite based on the MA-rXRPD data. A larger height indicates a smaller to no measured difference in depth between hydrocerussite and cerussite (and thus the presence of a homogeneous lead white mixture at the surface), while a lower height indicates the presence of a larger difference between hydrocerussite and cerussite (and thus the presence of a hydrocerussite-rich layer below a cerussite-rich layer).

Table 1. Overview of the $w_{HC}/(w_{HC}+ w_C)$ ratios for every layer (or set of layers) analyzed with μ-XRPD, MA-tXRPD (transmission), and MA-rXRPD (reflection). For MA-XRPD, an error of ±2σ is used; for μ-XRPD, a relative uncertainty value of ±10% is cited (see Materials and Methods).

Area	Technique	Layer(s)	$w_{HC}/(w_{HC} + w_C)$
Bright flesh tones	μ-XRPD	Upper (a_3)	0.65 ± 0.07
		Lower (a_4)	0.79 ± 0.08
		Ground (b_1)	—
	MA-tXRPD	All layers	0.75 ± 0.05
	MA-rXRPD	Superficial	0.65 ± 0.06
Shadow flesh tones	μ-XRPD	Upper (a_1)	0.48 ± 0.05
		Lower (a_2)	—
		Ground (b_2)	0.83 ± 0.08
	MA-tXRPD	All layers	0.82 ± 0.06
	MA-rXRPD	Superficial	0.37 ± 0.20
Background	MA-tXRPD	All layers	0.88 ± 0.04
	MA-rXRPD	Superficial	0.37 ± 0.20

In the shadow tones of the face, a lead white top layer of $w_{HC}/(w_{HC} + w_C) = 0.37 \pm 0.20$ can be distinguished by means of MA-rXRPD, while MA-tXRPD provides a ratio of 0.82 ± 0.06 for the entire stratigraphy. This latter ratio is similar to that of the ground layer, indicating that the upper cerussite-rich layer must be thin. This is confirmed by the μ-XRPD analysis (Fig. 2). Given that the typical $w_{HC}/(w_{HC} + w_C)$ ratio for lead white obtained from a 17th century stack synthesis is approximately 0.70, the presence of this thin cerussite-rich paint layer is noteworthy (*6*).

In the literature, two hypotheses have been proposed through which enrichment of cerussite can take place in lead white pigments: Either a longer corrosion time was used during the synthesis of lead white (allowing for the conversion of hydrocerussite to cerussite) or a postsynthesis treatment of the lead white in an acidic environment has taken place (*6*). Despite the fact that a hydrocerussite-rich paint is easier to apply and creates a sharper impasto, Vermeer seems to have consciously used a cerussite-rich paint (*25*).

The most important factor in determining the optical properties of lead white paint, however, is the particle size, which is strongly linked to the opacity of the paint. A larger particle size ensures a higher covering power and a higher opacity, while a smaller particle size achieves a more transparent effect. One method used in the 17th century to allow for particle size selection involves washing and decanting (*25*). A different 17th century procedure for obtaining lead white paint with a small particle size was an acidic postsynthesis treatment carried out by washing and grinding the pigment in vinegar (*6*). Preexisting crystallites are dissolved and recrystallized as small cerussite particles. This process not only causes a reduction in the particle size but it also increases the proportion of cerussite due to the instability of hydrocerussite in an acidic environment. As the proportion of hydrocerussite decreases, so do the opacity and brightness, albeit slightly. Hydrocerussite crystals, shaped like hexagonal platelets, recline better under brush strokes than the elongated rhombohedra cerussite crystals, forming a reflective layer of similarly oriented platelets. This results in a higher covering power of the pigment and, consequently, in a (slightly) higher opacity of hydrocerussite-rich paint (*26*, *27*). The combination of these two effects may have motivated Vermeer to use a cerussite-rich paint to accentuate the contrast between the darker, cerussite-rich zones and the brighter, hydrocerussite-rich areas of the painting. Previous analysis of cross sections from the clothing has also indicated that Vermeer applied a thick dark underlayer and a thin transparent upper layer in the dark areas, while in the bright areas, he made use of a thin dark underlayer and a thick opaque upper layer (*28*). It is well known that Vermeer intentionally varied his underlayers to achieve a variety of color effects in his paintings, explaining his use of transparent materials at the surface (*29*). A stratigraphy of all the lead-containing layers in the shadow areas is suggested in Fig. 5A.

A similar hypothesis can be suggested for how Vermeer created the dark background. Besides the ground layer, a small amount of lead white in the top layer [with $w_{HC}/(w_{HC} + w_C) = 0.37 \pm 0.20$] is present in this area along with the secondary formation product palmierite. These findings align well with an earlier paint sample examination of *Girl with a Pearl Earring*, in which it was found that the background areas consist of a superficial transparent glaze layer, containing organic dyes (indigo and weld), chalk, alum, lead white, and red ochre, on top of a dark underpaint (*28*). It is assumed that Vermeer originally created a translucent dark green background, made darker and given depth by the underpaint. This would explain

the presence of the cerussite-rich lead white in the glaze layer, which is associated with more translucent optical properties. A possible lead white stratigraphy for the background area is suggested in Fig. 5A.

In the bright flesh tones of the *Girl* (Fig. 5A), MA-rXRPD confirms the presence of a top layer with a lead white ratio of 0.65 ± 0.06 (Fig. 3G, red curve). The MA-tXRPD analysis yields a ratio of 0.75 ± 0.06. A logical conclusion based on these data would be that the paint stratigraphy consists of a layer with $w_{HC}/(w_{HC} + w_C) = 0.65$ on top of one with $w_{HC}/(w_{HC} + w_C) = 0.88$. The μ-XRPD analysis, however, revealed the presence of a third layer, in between the top (pink) and ground layers, with a similar lead white ratio as the ground layer in the absence of calcite (Fig. 5A).

Figure 5B highlights the spatial correlation between the hydrocerussite/cerussite ratio in the upper paint layer(s) (indicated by a false color range) and the average depth difference between hydrocerussite and cerussite, both types of information obtained with MA-rXRPD, (indicated by the height of the relief). In the elevated areas, the relative depth is zero, which means that hydrocerussite and cerussite are mixed homogeneously and present at the surface. A hydrocerussite-rich lead white paint has been applied in these areas. In the low-lying areas, which indicate a large difference in depth between hydrocerussite and cerussite, a cerussite-rich lead white paint has been applied on top of a hydrocerussite-rich layer. These observations are fully consistent with the stratigraphy and the μ-XRPD maps of hydrocerussite and cerussite shown in Fig. 2.

As already pointed out, an important limitation of MA-XRPD in its present form is that it is unable to resolve complex layer sequences into individual contributions. The top layer can be analyzed directly in reflection mode, but in transmission mode, only information on the sum of all the layers becomes available. This highlights the need for other, more discriminatory techniques such as μ-XRPD to differentiate between individual layers. The question remains, of course, why Vermeer decided to use two different types of hydrocerussite-rich paint in the bright part of the face. One possible explanation is that Vermeer opted for a higher-quality lead white for the surface paint by using a pigment that was more intensely washed and ground after its synthesis, increasing the proportion of cerussite.

Conclusion

In this study, the information obtained with noninvasive and in situ MA-XRPD in transmission and reflection modes was used to propose a stratigraphy for the different lead white layers present in the various regions of *Girl with a Pearl Earring*, providing both qualitative and quantitative information on the macroscopic scale. An accurate and representative estimation of three different types of lead white used by Vermeer was obtained using MA-XRPD. To verify and complement the findings from the macroscopic analysis, we analyzed several microscopic cross sections with μ-XRPD. While μ-XRPD provides less accurate and representative quantitative information, it proved necessary in revealing additional layers that could not be detected with MA-XRPD for complex multilayered paint systems. Consequently, a combination of both μ-XRPD and MA-XRPD proved to be highly useful in proposing a hypothesis about how Vermeer used different types of lead white in *Girl with a Pearl Earring*.

At least four distinct types of lead white paint have been used in the analyzed areas of *Girl with a Pearl Earring*. The ground layer consists of lead white paint with a hydrocerussite-rich composition in a matrix of chalk. The bright parts of the face contain two hydrocerussite-rich paints: one hydrocerussite-rich paint mixed with vermillion and one very hydrocerussite-rich paint in the layer below. Last, in the shadow areas and in the background, Vermeer used a transparent lead white paint rich in cerussite, presumably to induce a sense of contrast with the bright parts of the painting. This suggests that Vermeer was well aware of the distinctive optical properties of various types of lead white and was highly discriminating in using them in his paintings.

MATERIALS AND METHODS

MA-XRF imaging

MA-XRF maps of the entire painting were collected in two scan sessions using the Bruker M6 Jetstream (*11*). The instrument consists of a measuring head equipped with a 30 W rhodium-target microfocus x-ray tube, a polycapillary lens, and an XFlash silicon drift detector with a beryllium window (energy resolution of <145 eV at Mn-K_α). By slowly moving the measuring head on the XY motorized stage, the painting was scanned pixel by pixel, line by line. By recording the emitted x-ray fluorescence radiation, the chemical elements present in the paint (associated with specific pigments) can be identified. With the Bruker M6, only elements heavier than silicon can be detected. Scans were carried out at 50 kV and a current of 600 μA, with a 400-μm step size and a dwell time of 125 ms. The distance between the scanning head and the paint surface was set at c. 1 cm, corresponding to an x-ray spot size of c. 300 μm. All data were collected with the Bruker M6 Jetstream software package. The acquired data cubes were then exported as raw files and processed and stitched using PyMca and the in-house developed Datamuncher software (*30*, *31*).

Reflectance imaging spectroscopy

Infrared hyperspectral reflectance image cubes were collected with an optimized whisk broom line-scanning imaging spectrometer (SOC720, Surface Optics Corporation) that uses an InGaAs array (SUI 640SDV, Sensors Unlimited) operating from 967 to 1680 nm with 3.4-nm sampling at an integration time of 33 ms per line (*13*). The painting was illuminated with two 125 W 3000 K halogen lamps whose voltage was regulated with a rheostat such that the effective color temperature was approximately 1000 K, giving a light level of approximately 700 lux at the artwork. The image cubes were dark-corrected, flat-fielded, and calibrated to apparent reflectance using diffuse reflectance standards (Labsphere Inc.). The calibrated image cubes were spatially registered using a point-based algorithm, and the resulting spatial sampling was 0.17 mm per pixel (*13*, *32*). The image cubes were processed using MATLAB custom software and ENVI.

MA-XRPD imaging

The imaging experiments on the painting *Girl with the Pearl Earring* were carried out using a laboratory scanning MA-XRPD/MA-XRF scanner, both in reflection and in transmission mode. In transmission mode, a high-brilliance low-power x-ray microsource (44 W; IμS-Ag^{HB}, Incoatec GmbH, Germany) was used to generate a monochromatic Ag-K_α (22.16 keV) x-ray beam with a photon flux of 1.1×10^7 photons s^{-1}; a focal diameter of 112 (3) μm, a focal distance of 22 (1) cm, and a divergence of 3.8 (3) mrad. Diffraction signals were recorded using a 2D diffraction detector (PILATUS 200K, DECTRIS Ltd., Germany). The detector was placed perpendicular to the x-ray source with the painting in between. The distance between the x-ray source and the

PILATUS detector was set at 22 cm to attain the best possible angular resolution. The distance between the painting and the detector was set at 11 cm, ensuring a sufficiently wide coverage of the angular range. At a distance of 11 cm between the x-ray source and the painting, a beam diameter of approximately 0.4 mm was obtained. Calibration of the setup was performed with a hydrocerussite paint layer on a mock-up panel. The diffraction data collected in transmission mode were corrected for attenuation effects.

In reflection mode, a monochromatic Cu-K_α (8.04 keV) x-ray source was used. Because of geometrical limitations dictated by the dimensions of the x-ray source, it is undesirable to use an incident angle lower than 10°. The lower primary energy of the Cu source causes diffraction signals to shift toward higher 2θ angles. Low-energy x-rays were also more easily attenuated by the sample, rendering the scanner more sensitive for superficial phenomena. This x-ray source generates a photon flux of 2.9×10^8, has a focal diameter of 142 (2) μm, a focal distance of 20 (1) cm, and a divergence of 2.4 (1) mrad. The painting was placed at a distance of 20 cm from the x-ray source, while the distance between the painting and area detector was <0.5 cm. An incident angle of 10° was chosen to maximize the sensitivity for superficial compounds, leading to a beam with an elliptical footprint of approximately 1×0.2 mm^2. The PILATUS 200K detector was positioned on the same side of the painting as the x-ray source and at an angle of 40° with the painting surface. To account for topographical variations and curvatures on the painting surface, a laser distance sensor (Baumer Hold., CH) was used to automatically adjust the distance between the x-ray source and the painting for every point of the scan. Calibration of the setup was performed with a calcite paint layer on a mock-up panel.

In both geometries, x-ray fluorescence data can be simultaneously acquired by means of a Vortex silicon drift detector (Hitachi, Japan). A set of three motor stages (25 cm × 10 cm × 10 cm; Newport Corp., USA) are responsible for the movements during the scanning procedure. The x-ray source, PILATUS 200K detector, and Vortex detector were placed on a motorized platform, capable of moving the setup in the *XY* plane. The artwork was placed on a motorized easel, capable of moving the painting in the vertical (*Z*) direction.

The regions scanned on the painting in reflection and transmission modes are shown in Fig. 1A. In reflection mode, an area encompassing the entirety of the *Girl*'s face (200 mm × 224 mm) was scanned with an exposure time of 10 s point^{-1} and a step size of 2 mm × 2 mm, chosen larger than the actual beam size (1 mm × 0.2 mm) because of time constraints. In transmission mode, a smaller area (49.5 mm × 99.9 mm) was scanned with an exposure time of 10 s point^{-1} but with a reduced step size of 0.9 mm × 0.9 mm to attain a better spatial resolution.

Microsample analysis

Microscopic paint samples were collected from a light, pink flesh tone (forehead, sample X40) and a shadow tone (cheek, sample X39) from the *Girl*'s face to investigate stylistic and chemical differences. The paint samples were embedded in Technovit 2000 LC mounting resin (Heraeus Kulzer GmbH, Germany) and polished using a sample holder and Micromesh sheets up to grade 12000 (Micro-Surface Finishing Products Inc., Wilton, Iowa, USA) (*33*). A Zeiss Axio Imager.A2m microscope equipped with a Zeiss AxioCam MRc5 digital camera was used to examine the polished cross sections, before scanning electron microscopy–energy-dispersive x-ray analysis.

Synchrotron μ-XRPD

To gain more insight into the lead white stratigraphy of the painting, the two cross-sectioned samples (described above) were analyzed with μ-XRPD. The samples were analyzed at beamline P06 (PETRA III, DESY, Germany), a hard x-ray micro- and nanoprobe beamline suited for XRPD imaging experiments on the microscale. A Kirkpatrick-Baez optical system focuses the beam to a diameter of 0.5 μm and a flux of 10^{10} photons s^{-1} with a primary energy of 21 keV. The samples were placed in a sample holder that could be moved in the *XYZ* dimensions across several millimeters. An EIGER X 4M detector (DECTRIS Ltd., Germany) was used to collect the diffraction signals. The sample was placed at a distance of 18 cm in front of the detector, ensuring a sufficiently wide angular range. The collected diffraction data were corrected for attenuation effects.

XRPD data processing

The in-house developed software package XRDUA was used for the processing of all XRPD data. XRDUA provides the necessary tools for extracting crystalline-specific distributions from the large number of 2D diffraction patterns obtained during XRPD imaging experiments (*34*). The procedure to obtain compound-specific images from raw diffraction data is visualized in fig. S4. The acquired diffraction patterns were converted into 1D diffractograms by means of azimuthal integration after which the crystalline phases present in the diffractogram were identified. After integration, whole-pattern fitting was performed on the 1D diffractograms using a Rietveld model containing all the identified crystalline phases. The structural information was obtained from the American Mineralogist Crystal Structure Database (*35*). The relative positions and intensities of the diffraction peaks for every compound were kept fixed during the fitting, while the angle-independent parameter *W* of the Caglioti width function was used to model the peak width. Refined values for the scaling, displacement, and width parameters were obtained for each compound. The intensity scaling parameters obtained in each point of the image were used to visualize the spatial distribution of the different compounds (fig. S4). A more detailed explanation of the modeling procedure and the functionalities of XRDUA is offered elsewhere (*34*, *36*). Weight fractions were calculated using the aforementioned scaling parameters (fig. S4). The 2D distributions shown throughout this work are either based on the global scaling factor or the weight fraction data obtained from this fitting procedure. For the average μ-XRPD weight ratios, an estimated error of ±10% was used on the basis of the analysis of model samples with a known composition and the SD calculated for different microscopic areas within the same cross-sectional layer. These model samples were created by mixing known amounts of hydrocerussite and cerussite into a homogeneous powder, after which the aforementioned fitting procedure was applied to calculate the weight ratios. For the average weight ratios obtained with MA-XRPD, an error of ±2σ, derived from the Gaussian profiles used in the histograms, was used.

SUPPLEMENTARY MATERIALS

Supplementary material for this article is available at http://advances.sciencemag.org/cgi/content/full/5/8/eaax1975/DC1

Fig. S1. Overview of the MA-XRPD scanning instrument.

Fig. S2. NIR reflectance spectra for cerussite (lead carbonate powder) and hydrocerussite (lead white cremnitz).

Fig. S3. Extracting depth information with MA-XRPD.

Fig. S4. XRPD data treatment procedure.

Table S1. Overview of the scans performed with μ-XRPD and MA-XRPD.

REFERENCES AND NOTES

1. J. Wadum, Contours of Vermeer, in *Vermeer Studies*, I. Gaskell, M. Jonker, Eds. (Studies in the History of Art, National Gallery of Art, 1998), pp 201–223.
2. M. Gifford, Painting light: Recent observations on Vermeer's technique, in *Vermeer Studies*, I. Gaskell, M. Jonker, Eds. (Studies in the History of Art, National Gallery of Art, 1998), pp 184–199.
3. R. J. Gettens, H. Kühn, W. T. Chase, Lead White. *Stud. Conserv.* **12**, 125–139 (1967).
4. R. Harley, *Artists Pigments c. 1600–1835: A Study in English Documentary Sources* (Butterworth Scientific, ed. 2, 1982).
5. E. Welcomme, P. Walter, E. Van Elslande, G. Tsoucaris, Investigation of white pigments used as make-up during the Greco-Roman period. *Appl. Phys. A.* **83**, 551–556 (2006).
6. V. Gonzalez, G. Wallez, T. Calligaro, M. Cotte, W. De Nolf, M. Eveno, E. Ravaud, M. Menu, Synchrotron-based high angle resolution and high lateral resolution X-ray diffraction: Revealing lead white pigment qualities in old masters paintings. *Anal. Chem.* **89**, 13203–13211 (2017).
7. H. Kühn, A study of the pigments and the grounds used by Jan Vermeer. *Rep. Stud. Hist. Art* **2**, 154–175 (1968).
8. E. Welcomme, P. Walter, J.-L. Bleuet, E. Hodeau, E. Dooryhee, P. Martinetto, M. Menu, Classification of lead white pigments using synchrotron radiation micro X-Ray diffraction. *Appl. Phys. A* **89**, 825–832 (2007).
9. V. Gonzalez, T. Calligaro, G. Wallez, M. Eveno, K. Toussaint, M. Menu, Composition and microstructure of the lead white pigment in Masters paintings using HR Synchrotron XRD. *Microchem. J.* **125**, 43–49 (2016).
10. M. Alfeld, K. Janssens, J. Dik, W. De Nolf, G. Van der Snickt, Optimization of mobile scanning macro-XRF systems for the in situ investigation of historical paintings. *J. Anal. At. Spectrom* **26**, 899–909 (2011).
11. M. Alfeld, J. V. Pedroso, M. van Eikema Hommes, G. Van der Snickt, G. Tauber, J. Blaas, M. Haschke, K. Erler, J. Dik, K. Janssens, A mobile instrument for in situ scanning macro-XRF investigation of historical paintings. *J. Anal. At. Spectrom* **28**, 760–767 (2013).
12. S. Legrand, M. Alfeld, F. Vanmeert, W. De Nolf, K. Janssens, Macroscopic Fourier transform infrared scanning in reflection mode (MA-RFTIR), a new tool for chemical imaging of cultural heritage artefacts in the mid-infrared range. *Analyst* **139**, 2489–2498 (2014).
13. K. A. Dooley, D. M. Conover, L. D. Glinsman, J. K. Delaney, Complementary standoff chemical imaging to map and identify artist materials in an early Italian Renaissance panel painting. *Angew. Chem. Int. Ed.* **53**, 13775–13779 (2014).
14. M. H. Brooker, S. Sunder, P. Taylor, V. J. Lopata, Infrared and Raman spectra and X-ray diffraction studies of solid lead(II) carbonates. *Can. J. Chem.* **61**, 494–502 (2011).
15. G. Chiari, P. C. Sarrazin, M. Gailhanou, Portable XRD/XRF instrumentation for the study of works of art. *Powder Diffr.* **23**, 175–186 (2008).
16. I. Nakai, A. Yoshinari, Portable X-ray powder diffractometer for the analysis of art and archaeological materials. *Appl. Phys. A* **106**, 279–293 (2012).
17. W. De Nolf, J. Dik, A. Wallert, K. Janssens, G. Van der Snickt, High-energy X-ray powder diffraction for the imaging of (hidden) paintings. *J. Anal. At. Spectrom* **26**, 910–916 (2011).
18. F. Vanmeert, W. De Nolf, S. De Meyer, J. Dik, K. Janssens, Macroscopic X-ray powder diffraction scanning, a new method for highly selective chemical imaging of works of art: Instrument optimization. *Anal. Chem.* **90**, 6436–6444 (2018).
19. F. Vanmeert, E. Hendriks, G. Van der Snickt, L. Monico, J. Dik, K. Janssens, Chemical mapping by macroscopic X-ray powder diffraction of Van Gogh's *Sunflowers*: Identification of areas with higher degradation risk. *Angew. Chem. Int. Ed. Engl.* **57**, 7418–7422 (2018).
20. F. Vanmeert, W. De Nolf, J. Dik, K. Janssens, Macroscopic X-ray powder diffraction scanning: Possibilities for quantitative and depth-selective parchment analysis. *Anal. Chem.* **90**, 6445–6452 (2018).
21. S. De Meyer, F. Vanmeert, K. Janssens, P. Storme, A Mobile Scanner for XRPD-Imaging of Paintings in Transmission and Reflection Geometry, in *6th Interdisciplinary ALMA conference*, Academy of Fine Arts in Prague, Brno, 2017.
22. M. Bacci, M. Picollo, G. Trumpy, M. Tsukada, D. Kunzelman, Non-invasive identification of white pigments on 20th century oil paintings by using fiber optic reflectance spectroscopy. *J. Am. Inst. Conservat.* **46**, 27–37 (2007).
23. A. Van Loon, P. Noble, J. J. Boon, White hazes and surface crusts in Rembrandt's *Homer* and related paintings, in *ICOM Committee for Conservation, 16th Triennial Meeting*; Lisbon, 26 to 30 2011.
24. J. J. Boon, Chemistry underneath the painting surface: Palmierite formation in/on a painting by Johannes Vermeer and by Jacob Jordaens using laboratory- and synchrotron-aided spectroscopic methods. *J. Micro. Microanal.* **19**, 1408–1409 (2013).
25. M. J. N. Stols-Witlox, L. Megens, L. Carlyle, "To prepare white excellent...": Reconstructions investigating the influence of washing, grinding and decanting of stack-process lead white on pigment composition and particle size, in *The Artist's Process: Technology and Interpretation*, S. Eyb-Green, J. H. Townsend, M. Clarke, J. Nadolny, S. Kroustallis, Eds. (Archetype London, 2012), pp 112–129.
26. T. Shahwan, B. Zunbul, D. Akar, Study of the scavenging behavior and structural changes accompanying the interaction of aqueous Pb^{2+} and Sr^{2+} ions with calcite. *Geochem. J.* **39**, 317–326 (2005).
27. A. Sánchez-Navas, O. López-Cruz, N. Velilla, I. Vidal, Crystal growth of lead carbonates: Influence of the medium and relationship between structure and habit. *J. Cryst. Growth* **376**, 1–10 (2013).
28. K. M. Groen, I. D. Van der Werf, K. J. Van den Berg, J. J. Boon, Scientific Examination of Vermeer's "Girl with a Pearl Earring" (Dutch Portraiture), in *Vermeer Studies*, I. Gaskell, M. Jonker, Eds. (Studies in the History of Art, National Gallery of Art, 1998), pp 169–183.
29. N. Costaras, A Study of the Materials and Techniques of Johannes Vermeer, in *Vermeer Studies*, I. Gaskell, M. Jonker, Eds. (Studies in the History of Art, National Gallery of Art, 1998), pp 144–167.
30. M. Alfeld, K. Janssens, Strategies for processing mega-pixel X-ray fluorescence hyperspectral data: A case study on a version of Caravaggio's painting *Supper at Emmaus*. *J. Anal. At. Spectrom* **30**, 777–789 (2015).
31. V. A. Solé, E. Papillon, M. Cotte, P. Walter, J. Susini, A multiplatform code for the analysis of energy-dispersive X-ray fluorescence spectra. *Spectrochim. Acta Part B At. Spectrosc.* **62**, 63–68 (2007).
32. D. M. Conover, J. K. Delaney, M. H. Loew, Automatic Registration and Mosaicking of Technical Images of Old Master Paintings. *Appl. Phys. A.* **119**, 1567–1575 (2015).
33. A. Van Loon, K. Keune, J. J. Boon, Improving the Surface Quality of Paint Cross Sections for Imaging Analytical Studies with Specular Reflection FTIR and Static-SIMS, in *Proceedings of Art Conference on Nondestructive Testing and Microanalysis for the Diagnostics and Conservation of the Cultural and Environmental Heritage*, Lecce, 15 to 19 May 2005.
34. W. De Nolf, F. Vanmeert, K. Janssens, *XRDUA*: Crystalline phase distribution maps by two-dimensional scanning and tomographic (micro) X-ray powder diffraction. *J. Appl. Cryst.* **47**, 1107–1117 (2014).
35. R. T. Downs, M. Hall-Wallace, The American Mineralogist crystal structure database. *Am. Mineral.* **88**, 247–250 (2003).
36. W. De Nolf, Imaging of crystalline phase distributions by means of scanning and tomographic X-ray powder diffraction, thesis, University of Antwerp: Antwerp (2013).

Acknowledgments: We would like to thank the Mauritshuis and its staff for the collaboration. We acknowledge DESY (Hamburg, Germany), a member of the Helmholtz Association HGF, for the provision of experimental facilities and travel reimbursement. Parts of this research were carried out at PETRA III, and we would like to thank J. Garrevoet, M. Alfeld, and G. Falkenberg for assistance at beamline P06. The research leading to this result has been supported by the project CALIPSOplus under the Grant Agreement 730872 from the EU Framework Programme for Research and Innovation Horizon 2020. **Funding:** K.J. wishes to thank the Research Council of the University of Antwerp for financial support through GOA project SolarPaint. Also, FWO, Brussels is acknowledged for financial support through grants G056619N and G054719N. The support of InterReg programme Smart*Light is appreciated. **Competing interests:** The authors declare that they have no competing interests. **Author contributions:** Data acquisition/analysis was performed by S.D.M., F.V., R.V. and K.J. (MA-XRPD); K.D. and J.De. (NIR reflectance); A.V.L. (MA-XRF); S.D.M., V.G., F.V., and K.J. (μ-XRPD). A.V. coordinated the project along with G.V.D.S. and J.D. The manuscript was written by S.D.M. with input from K.J. and all other authors. All authors contributed to the manuscript. **Data and materials availability:** All data needed to evaluate the conclusions in the paper are present in the paper and/or the Supplementary Materials. Additional data related to this paper may be requested from the authors.

Submitted 1 March 2019
Accepted 31 July 2019
Published 30 August 2019
10.1126/sciadv.aax1975

Citation: S. De Meyer, F. Vanmeert, R. Vertongen, A. Van Loon, V. Gonzalez, J. Delaney, K. Dooley, J. Dik, G. Van der Snickt, A. Vandivere, K. Janssens, Macroscopic x-ray powder diffraction imaging reveals Vermeer's discriminating use of lead white pigments in *Girl with a Pearl Earring*. *Sci. Adv.* **5**, eaax1975 (2019).

Macroscopic x-ray powder diffraction imaging reveals Vermeer's discriminating use of lead white pigments in *Girl with a Pearl Earring*

S. De Meyer, F. Vanmeert, R. Vertongen, A. Van Loon, V. Gonzalez, J. Delaney, K. Dooley, J. Dik, G. Van der Snickt, A. Vandivere and K. Janssens

Sci Adv **5** (8), eaax1975.
DOI: 10.1126/sciadv.aax1975